Effects of photoacoustic measurements on a nanostructured ZnSe mechanically alloyed

2008 J. Phys.: Condens. Matter 20 465205

(http://iopscience.iop.org/0953-8984/20/46/465205)

J. Phys.: Condens. Matter **20** (2008) 465205 (8pp) doi:10.1088/0953-8984/20/46/465205

Effects of photoacoustic measurements on a nanostructured ZnSe mechanically alloyed

J Baltazar-Rodrigues[1], J C de Lima[2], C E M Campos[2] and T A Grandi[2]

[1] Departamento de Física, Universidade Estadual de Ponta Grossa-Pr, Campus de Uvaranas, CEP: 88040-900-Ponta Grossa, Paraná, Brazil
[2] Departamento de Física, Universidade Federal de Santa Catarina, Campus Universitário, Trindade, CP 476. CEP: 88040-900-Florianópolis, Santa Catarina, Brazil

Received 4 June 2008, in final form 26 September 2008
Published 21 October 2008
Online at stacks.iop.org/JPhysCM/20/465205

Abstract
Zinc-blende ZnSe powder, with particles containing nanometric grains, was prepared using the mechanical alloying technique, from an equiatomic mixture of elemental Zn and Se powders. An important interfacial component was observed in the as-milled powder, which affects its thermal and optical properties. In order to obtain a high-quality zinc-blende ZnSe powder an annealing process was applied. The structural properties of both as-milled and annealed powders were characterized by an x-ray diffraction technique. The effects of defect centers on the optical band gap of both as-milled and annealed zinc-blende ZnSe powders were studied through optical absorbance measurements. The results showed a substantial broadening and a shift of the band gap energy to lower values in the as-milled powder, while for the annealed sample no effects were observed. For the annealed sample, the measured band gap energy value is in good agreement with those reported in the literature. A sequence of photoacoustic absorption measurements of the as-milled ZnSe sample showed that the absorbed energy promotes a structural relaxation. This relaxation causes a change in the heat transfer mechanism from thermal diffusion to thermoelastic bending and a reduction in the thermal diffusivity values. Similar measurements of the annealed nanostructured ZnSe sample showed the thermal diffusivity value to have a high degree of stability, and to be in good agreement with values reported in the literature.

1. Introduction

Materials having a microstructure formed by particles containing grains or crystallites of nanometer dimensions (hereafter called nanostructured materials) are being widely investigated due to their potential for new technological applications as well as their scientific interest. As an example, recent researches on semiconductor quantum dots have demonstrated that to reach quantum size effects it is necessary to synthesize nanometer-size crystallites smaller than the exciton (electron–hole pair) Bohr diameter (≈9 nm) [1].

From the structural point of view, nanostructured materials are considered to be composed of two components; one crystalline of nanometer dimensions, which preserves the bulk crystal characteristics, and the other interfacial, composed of defect centers (grain boundaries, interphase boundaries, dislocations, etc). The first one shows strained crystal lattice regions, while the interfacial component has caused controversy in the literature. Gleiter [2] describes it based on a gaseous model, which other authors do not agree with [3]. The number of atoms in both components is similar [3] and, thus, the nanostructured material properties are strongly dependent on the atomic configurations present in the interfacial component. From a technological point of view, the manipulation of the interfacial component may offer the possibility to design new materials with physical properties for specific applications [2, 3].

The zinc selenide (ZnSe) alloy is an important II–VI semiconductor with a wide band gap (2.45 eV) [4]. Its doping makes it possible to change the wavelength of band-to-band

transitions permitting emission in the green, blue, or even UV, region of the light spectrum [5–7]. This compound is used as a material for luminescence, lasers, and infrared filter devices [5–7]. Nanostructured ZnSe can be synthesized by the following methods: arrested nucleation in glass [7–11], precipitation from sol–gel solutions [12], and entrapment in porous sites inside zeolite cavities [7], among others. All of these techniques, besides being expensive, are not entirely able to control the size of the nanoparticles obtained. This illustrates the difficulties encountered in obtaining the ZnSe alloy in nanostructured form.

Mechanical alloying (MA) is an efficient technique to synthesize many unique materials, such as nanostructured crystalline, amorphous alloys and metastable solid solution phases [13–15]. This technique has many advantages including processing at low temperatures, easy composition control, inexpensive equipment and the possibility of scaling up. Its disadvantage is the contamination of milled powder by the milling media, and possibly by the milling atmosphere used. MA has also been used to produce commercially important alloys in a much simpler way, in particular, those whose components have a very high melting point [1], causing difficulties in the use of techniques based on fusion. For some systems, MA permits an increase in the limit of solubility in solid solutions [13]. It has been applied to mixtures composed of immiscible elements [11–13, 16], allowing the formation of unstable solid solutions in equilibrium conditions. However, the physical mechanisms involved are still not well understood. For industrial applications, a better understanding of these mechanisms is required.

Due to the technological importance of the Zn–Se system and nanostructured materials, our research is focused on establishing a method to produce a high-quality nanostructured ZnSe powder by MA. However, the MA technique produces materials containing a high concentration of defect centers, which before any treatment are commonly called as-milled. A high concentration of defect centers causes instability in the thermal and optical properties. Thus, to produce a high-quality nanostructured ZnSe powder the configuration of the defect centers in both interfacial and crystalline components must be stabilized. This can be achieved through a controlled annealing process.

On the other hand, it is very difficult to follow the evolution of the interfacial component with annealing because its contribution to the XRD pattern appears as an increase in the background. Thus, other techniques sensitive to the defect concentration such as optical absorbance and photoacoustic absorption (PAS) spectroscopy must be used. However, it is well known that the high defect concentration causes a broadening in the optical absorbance spectrum making it difficult to evaluate correctly the energy band gap. The PAS is a photothermal phenomenon that has been widely used to study the thermo-optical properties of materials. Furthermore, PAS is extremely dependent on the effects of compositional and microstructural variables as well as processing conditions. Due to their characteristics, the optical absorbance and PAS are appropriate tools to investigate the effect of the interfacial component in the optical and thermal properties of the as-milled and annealed nanostructured ZnSe powders mechanically alloyed [17, 18].

This paper reports the results obtained through optical absorbance and PAS measurements of the as-milled and annealed ZnSe samples. The effects of the annealing process on the as-milled ZnSe powder are also reported.

2. Theoretical background

2.1. Optical absorbance measurement and determination of the band gap energy

A fundamental property of semiconductor materials is the optical band gap energy, the forbidden energy region located between the filled valence and empty conduction bands. Optical excitation of electrons across the optical band gap is strongly allowed, producing an abrupt increase in the absorption spectrum at the wavelength corresponding to the optical band gap energy. This feature in the optical spectrum is known as the optical-absorption edge. For a semiconductor material with a band gap energy value between 0.5 and 3 eV, the optical-absorption edge can be easily measured by means of conventional optical spectroscopy.

The most direct way to obtain the optical band gap energy value is to simply determine the wavelength at which the extrapolations of the baseline and the absorption edge cross [4]. However, when the material is in the form of a nanostructured powder some problems arise. Defects and impurities introduce trap states just below the conduction band or just above the valence band. Absorption by defect and impurity states causes a smearing of the absorption edge [4]. Particles containing nanometer-sized crystallites cause a shift in the optical band gap value [22]. The shift value decreases as the crystallite size increases. Thus, in an absorbance measurement, the combination of these effects gives an average edge, inhibiting the determination of the optical band gap energy value and making it less precise.

The optical band gap energy value can be obtained by a McLean analysis of the absorption edge through the equation [4].

$$\alpha h\upsilon = (h\upsilon - E_g + E_p)^{1/n}, \tag{1}$$

where α is the absorption coefficient, E_g is the band gap, E_p is the phonon energy for indirect transitions, h is Planck's constant and υ is the frequency of the incident beam. The analysis consists of fitting the absorption edge to equation (5) and determining the experimental values for E_g and n. A value of $n = 2$ implies a direct allowed transition; $n = 2/3$ implies a direct forbidden transition; $n = 1/2$ implies an indirect allowed transition; $n = 1/3$ implies an indirect forbidden transition.

The relationship between the absorbance A, absorption coefficient α and thickness d of a sample is given by [23]

$$\alpha = \frac{A}{d}. \tag{2}$$

For absorbance measurement of powders, the polycrystalline or amorphous sample is dispersed into a powder support, such as KBr, and the mixture is pressed into the form of

a pellet. In this case, the thickness d and absorption coefficient α of the sample are no longer known. Thus, equation (1) must be modified to

$$Ah\upsilon = C(h\upsilon - E_g + E_p)^{1/n}. \quad (3)$$

Here, C represents the thickness of the sample and is a parameter to be included in the fitting procedure.

2.2. Open photoacoustic cell measurement and determination of the thermal diffusivity parameter of semiconductor materials

Thermal diffusivity is defined as $\alpha_s = k/\rho c$, where k is the thermal conductivity, ρ the mass density and c the specific heat. It is an important physical parameter due not only to its intrinsic physical interest but also its use in the modeling and designing of technological devices based on semiconductor materials. Physically, the inverse of α_s is a measure of the time required to establish thermal equilibrium in a given material. Like the optical-absorption coefficient, its value is different for each material. Furthermore, the thermal diffusivity is also known to be strongly dependent on the effects of compositional and microstructural variables [19], as well as processing conditions [17]. Thus, an appropriate strategy to follow the structural changes in a binary mixture of Zn and Se submitted to the MA process is to measure the α_s parameter.

When a modulated light beam impinges on the material inside the photoacoustic gas cell, the absorbed light is converted into periodic heat and a PAS signal is created. The PAS signal dependence on the optical-absorption coefficient and the light-to-heat conversion efficiency allows us to obtain the nonthermal excitation efficiency, the photoinduced energy conversion processes, etc. The PAS signal is directly proportional to the light-to-heat conversion efficiency through nonradiative processes in the material [18]. For a thermally thick semiconductor sample, there are four processes that may contribute to the PAS signal:

(1) intraband nonradiative thermalization (thermal diffusion): when the photon-generated electrons relax down to the bottom of the band by creating phonons. The contribution of this process to the PAS signal decreases exponentially with the modulation frequency as

$$S = \frac{A}{f}\exp(-a\sqrt{f}) \quad (4)$$

where $a = l_s(\pi/\alpha_s)^{1/2}$, f is the modulation frequency, l_s is the sample thickness, and α_s its thermal diffusivity. The PAS signal phase shows a modulation frequency dependence of the type

$$\Phi_{ph} = \frac{\pi}{2} - af^{1/2}. \quad (5)$$

When this process is present, it occurs in the low frequency range;

(2) nonradiative bulk recombination: when nonradiative recombination of excess electron–hole pairs occurs after diffusion, it takes place over a distance $(D\tau)^{1/2}$. The contribution of this process to the PAS signal shows a modulation frequency dependence of the type $f^{-1.5}$. The thermal diffusivity α_s, carrier diffusion coefficient D, surface recombination velocity υ, and recombination time τ can be determined by fitting the PAS signal phase to the phase expression given by Pinto Neto [20],

$$\Phi_{ph} = \frac{\pi}{2} + \tan^{-1}\left[\frac{(bD/\upsilon)(\omega\tau_{eff}+1)}{(bD/\upsilon)(1-\omega\tau_{eff}) - 1 - (\omega\tau_{eff})^2}\right] \quad (6)$$

where $\tau_{eff} = \tau(D/\alpha_s - 1)$, $b = l_s(\pi f/\alpha_s)^{1/2}$, and $\omega = 2\pi f$. When present, it occurs in the high frequency range;

(3) nonradiative surface recombination: when nonradiative surface recombination of excess electron–hole pairs occurs, it takes place at the sample surface. The contribution of this process to the PAS signal shows a modulation frequency dependence of the type $f^{-1.0}$. Similarly to process (2), the α_s, D, υ, and τ parameters can be determined by fitting the PAS signal phase to the expression given by Pinto Neto [20]. When present, it occurs in the high frequency range after the nonradiative bulk recombination process; and

(4) thermoelastic bending: when a temperature gradient is generated within the sample, across its thickness, the thermoelastic bending process contributes to the PAS signal. This contribution shows a modulation frequency dependence of the type $f^{-1.0}$. The thermal diffusivity α_s can be determined by fitting the PAS signal phase to the expression

$$\Phi_{ph} = \phi_0 + \tan^{-1}\left[\frac{1}{a\sqrt{f}-1}\right] \quad (7)$$

where the constant a is the same as that defined for process (1). The PAS signal for processes (3) and (4) shows the same dependence on the modulation frequency. However, the PAS signal phases for each process have different dependences on the modulation frequency. Thus, an analysis of the PAS signal phase allows one to distinguish these processes and determine the α_s, D, υ, and τ parameters. The way to identify each process is given in the literature [21].

3. Experimental procedure

Two equiatomic batches of elemental selenium and zinc powders (purity $>$ 99.00%) were prepared. Each batch was sealed together with five steel balls with an average diameter of 11.5×10^{-3} m, inside a cylindrical steel container under argon atmosphere. The balls:powder weight ratio (BPR) was 6:1. The batches were milled for 10 h in a high-energy shaker mill (SPEX 8000). A ventilation system was used to keep the container temperature close to the ambient temperature. The milled powders, which had a dark brown color, were analyzed using the x-ray diffraction (XRD) technique. The XRD patterns were measured using a Rigaku powder diffractometer, Miniflex model, with Cu Kα radiation ($\lambda = 1.5418$ Å). In order to verify the stability of the as-milled powders, as well as the presence of unreacted components, differential scanning

calorimetry (DSC) was performed between 25 and 600 °C, with a heating rate of 10 °C min^{-1}, in a DSC cell, model TA 2010, manufactured by TA Instruments, Inc. Based on the DSC results, annealing was carried out on one batch. For this, a pellet of ZnSe was inserted into an evacuated quartz tube, which was maintained under low pressure in argon gas. The sample was annealed at 520 °C for 6 h, followed by air-cooling. After annealing, the ZnSe powder had the yellow color of commercial powder. The XRD pattern and DSC spectrum for the annealed sample showed a single zinc-blende nanostructured ZnSe phase.

The as-milled and annealed powders' particle sizes were measured using a Philips scanning electron microscopy, XL30 model, equipped with an energy dispersive x-ray (EDX) spectrometer and EDAX software. For as-milled and annealed powders the mean particle sizes were 2.11 and 1.36 μm, respectively. EDX analysis of the as-milled and annealed samples showed a low level of Fe contamination (<0.8 at.%) from the milling media, which was neglected.

In order to investigate the influence of the defect centers on the optical band gap, optical absorbance measurements were taken in an energy range of 1.2–3.4 eV, using a Perkin-Elmer spectrometer, Lambda 19 model.

The PAS measurements were taken using an open photoacoustic cell (OPC) configuration built in the laboratory. This OPC configuration consists of a 250 W quartz-tungsten-halogen QTH lamp stabilized by a Bentham 605 current power supply. The light beam, after being infrared-filtered by a water lens, is mechanically chopped by a Perkin-Elmer light chopper, model 197, and focused onto the sample. The sample is mounted directly onto the front sound inlet of an electret microphone [17]. The output voltage of the microphone is connected to a lock-in amplifier, which in turn is connected to a computer in order to record the PAS signal amplitude and phase as a function of the modulation frequency.

The samples for the PAS measurements were prepared by pressing the powder at the same pressure to form tiny circular pellets of 10 mm in diameter. The thicknesses of the as-milled and annealed samples were 590 and 570 μm, respectively. The PAS measurements were taken in the modulation frequency range of 10–270 Hz in order to achieve the thermally thick regime. The sequence of PAS measurements of the as-milled and annealed samples was taken with an interval of 24 h between them.

4. Results and discussion

4.1. XRD results for the as-milled and annealed ZnSe powder

Figure 1 shows the measured XRD patterns of the as-milled (a) and annealed (b) ZnSe powders. Results describing the structural characterization of both as-milled and annealed powders have been submitted for publication elsewhere. An excellent agreement between the patterns shown in figure 1 and that reported by de Lima *et al* [14] as well as with that given by the JCPDS card. No 37.1463 [24] was observed. The refined lattice parameter values for both as-milled and annealed samples were obtained using the Rietveld refinement

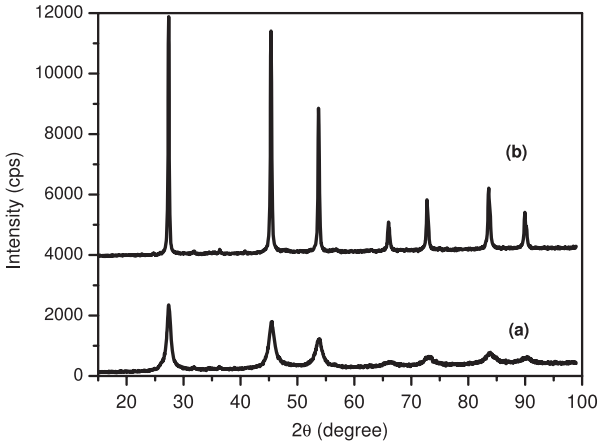

Figure 1. XRD patterns for nanostructured ZnSe powders: as-milled (a) and annealed (b).

method [25], and the values found were **a** = 5.643 Å and 5.655 Å, respectively. The difference between these values is attributed to an increase in the mean crystallite size and a decrease in the strains in the crystalline component, as well as the partial elimination of the interfacial component by annealing.

All the peaks on the XRD pattern for the as-milled ZnSe phase are enlarged, indicating a nanometric structure. The nanometric structure is formed by crystallites having dimensions of a few nanometers (from 2 up to 100 nm) [2]. The mean size of the crystallites can be satisfactorily estimated from the simulated XRD pattern taking into account the line broadening caused by both crystallite size and strain through the relationship [26]

$$\left(\frac{\beta_t \cos\theta}{K\lambda}\right)^2 = \frac{1}{d^2} + \sigma_p^2 \left(\frac{\sin\theta}{K\lambda}\right)^2, \qquad (8)$$

where θ is the diffraction angle, λ is the x-ray wavelength, β_t is the total broadening measured at the full-width at half-maximum (FWHM) of the peak in radians, d is the crystallite size, σ_p is the strain, and K is a constant dependent on the measurement conditions and on the definition of β_t and d (here K was assumed to be 0.91 as is usual in the Scherrer formula). Graphical linearization of the above relationship, i.e., the plotting of $\beta_t^2 \cos^2\theta/\lambda^2$ versus $\sin^2\theta/\lambda^2$, yields the mean crystallite size free of strain effects from the values of the intercept of the straight line obtained, as well as the strain obtained from the slope. The code DBWS 9807 generates the β_t and 2θ positions for all the simulated peaks. Considering these values in expression (8), the values found were $d \approx 9.0$ nm and $\sigma_p \approx 2.5\%$. On the other hand, on the XRD pattern of the annealed ZnSe sample all the peaks were narrow, indicating that the annealing process promoted grain growth and structural relaxation. However, all the peaks still show an enlarged base, suggesting that the nanometric structure was not completely eliminated by the annealing process. Thus, expression (8) above was also applied to the measured data for this sample, and the calculated values were $d \approx 33.0$ nm and $\sigma_p \approx 0.3\%$.

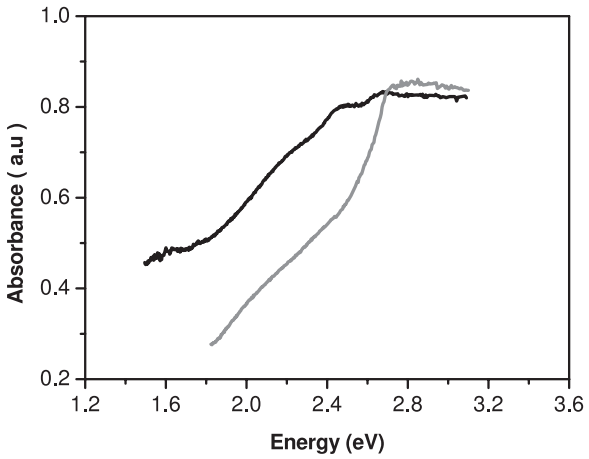

Figure 2. Absorbance spectra for nanostructured ZnSe powders: as-milled (black line) and annealed (gray line).

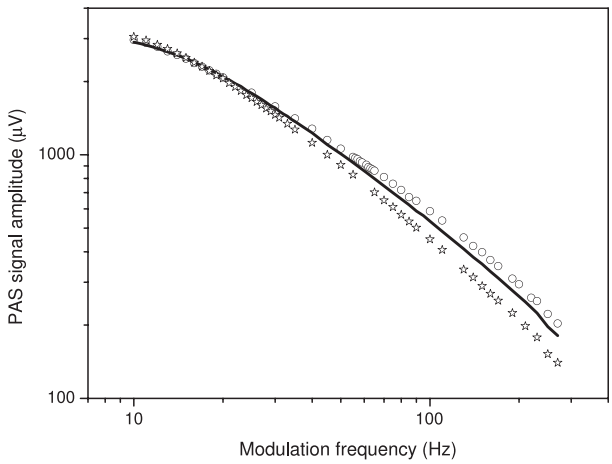

Figure 3. Sequence of PAS signal amplitude measurements of the as-milled nanostructured ZnSe powder. First measurement (open circles), second measurement (solid line), and third measurement (open stars).

A comparison between these values for the as-milled and annealed samples showed that the annealing process promoted a substantial reduction in the strain and stress as well as an increase of almost four times in the crystallite size.

4.2. Optical absorbance for the as-milled and annealed ZnSe powder

Figure 2 shows the absorbance spectra as a function of the light photon wavelength of the as-milled (curve a) and annealed (curve b) samples. From this figure one can see that the optical band gap corresponding to the as-milled sample (curve (a)) is very large due to the crystallite size of $d \approx 9.0$ nm and the strain value of $\sigma_p \approx 2.5\%$, as well as the substantial interfacial component. All of these features inhibit the precise determination of the optical band gap energy. Thus, the best estimated value for the band gap energy was $E_g \approx 1.72$ eV. On the other hand, the absorbance spectrum for the annealed ZnSe sample shows a narrow optical-absorption edge, confirming that the annealing process promoted grain growth and structural relaxation. The best fitting of experimental data to expression (3) above gave a band gap energy of $E_g \approx 2.47$ eV. This value shows an excellent agreement with that reported in the literature ($E_g \approx 2.45$ eV) [4]. The XRD and optical absorbance results show that to produce high-quality nanostructured ZnSe powder, the MA technique followed by an annealing process can be used.

4.3. OPC measurements of the as-milled and annealed ZnSe powder

Sankar and Ramachandran [27] reported a value of 1.01×10^{-5} m^2 s^{-1} for the thermal diffusivity of ZnSe crystal. This value has been used to calculate the characteristic frequency $f_c = \alpha_s/\pi \cdot l_s^2$, which defines the transition from a thermally thin regime ($f < f_c$) to a thermally thick regime ($f > f_c$). Since the thickness of our sample is 590 μm, a characteristic frequency of 9 Hz was calculated. Thus, the PAS data were acquired between 10 and 270 Hz, in order to achieve a thermally thick regime.

Figure 3 shows the PAS signal amplitude corresponding to the first three measurements of the as-milled sample. From this figure one can see a change in the signal amplitude with the sequence of measurements, especially between 25 and 100 Hz. As stated above, the contribution of the thermal diffusion mechanism to the PAS signal amplitude occurs between 10 and 20 Hz, followed by the presence of another mechanism. This is clearly shown by changes in the slope of these curves. Between 25 and 100 Hz, the PAS signal amplitudes show a modulation frequency dependence of the type $\approx f^{-1.0}$, which is characteristic of nonradiative surface recombination, the thermoelastic bending process or thermal dilation [28]. The thermal dilation process produces a signal, the phase of which is independent of the modulation frequency and equal to $-90°$. As will be shown in the next figure, this behavior is not observed, allowing us to disregard this heat transfer mechanism.

Figure 4 shows the PAS signal phase corresponding to the first three measurements of the as-milled sample. The open circle, thick solid line and open star curves describe the first, second and third measurement, respectively. The phase corresponding to the first measurement shows a discontinuity at the modulation frequency of 62 Hz, while for the second and third measurements this discontinuity is observed at 32 and 11 Hz, respectively. In order to understand the discontinuity shift to a lower modulation frequency with the sequence of measurements, it is necessary to understand the heat effects on the defect centers. In order to nonradiatively dissipate the absorbed energy, a large number of phonons have to be emitted simultaneously. The presence of defect states in the band gap significantly facilitates this process. As a result, heating predominantly occurs in the vicinity of the sites responsible for these states, selectively heating them to a temperature that may considerably exceed the average temperature [29]. Structural transformations may thus take place locally without relaxation of the complete structure. On the other hand, in a previous study [5], we reported structural changes in an ZnSe alloy with ageing (segregation of the

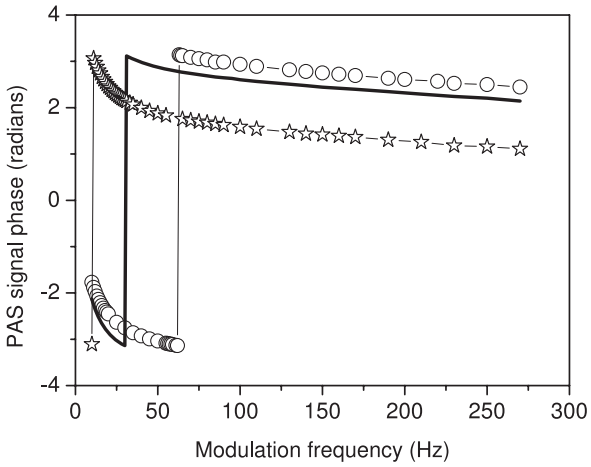

Figure 4. Sequence of PAS signal phase measurements of the as-milled nanostructured ZnSe powder. First measurement (open circles), second measurement (solid line), and third measurement (open stars).

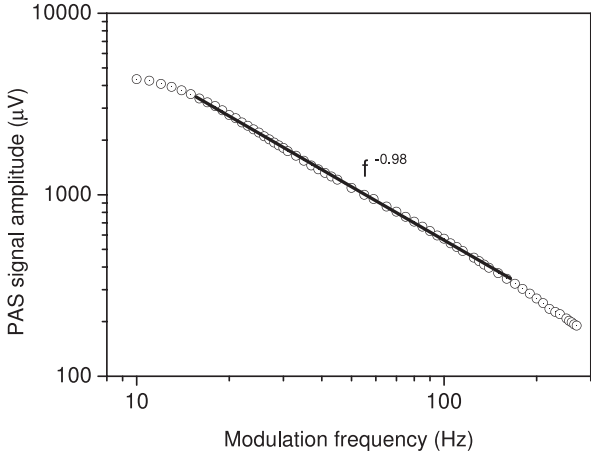

Figure 5. PAS signal amplitude for the annealed nanostructured ZnSe powder. The solid straight line shows the PAS signal amplitude dependence on the modulation frequency.

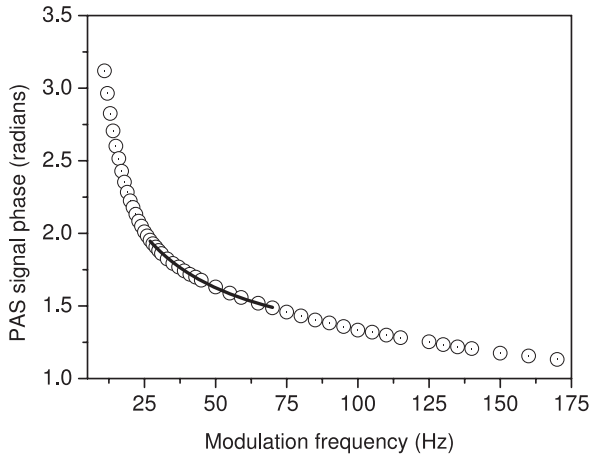

Figure 6. PAS signal phase measurement of the annealed nanostructured ZnSe powder. The solid line represents the fit of experimental data to equation (4).

hexagonal selenium phase). These previous results showed that the room temperature energy (≈0.025 eV) is sufficient to relax defect centers with low activation energy. Therefore, the absorbed energy in the PAS measurements promotes the structural relaxation of low activation energy defect centers. This assumption seems to be supported by the fact that the ZnSe sample shows a nanometric structure after an annealing process, which indicates the presence of high activation energy defect centers. Therefore, the relaxation process may be responsible for the discontinuity shift observed in figure 4.

The high number of states related to the defect centers in the optical band gap is corroborated by the absorbance spectrum for the as-milled sample (see figure 2). It is interesting to note that the PAS signal amplitude is not very sensitive to the heat effect on the defect centers as shown in the figure 3. On the other hand, the PAS signal phase is highly sensitive.

The phase inversion observed in figure 4 can be physically explained by the following statement: the thermoelastic bending mechanism is, generally, a non-dissipative process and is a result of the temperature gradient inside the sample, normal to the side of the greatest sample dimension [28]. Due to the fact that sample face exposed to the light is hotter than the other face mounted in the electret microphone inlet used as the photoacoustic cell, the temperature gradient promotes a thermal expansion of the sample face exposed to the light and a contraction of the other one, a fact that causes a bending of the sample. This bending reduces the pressure in the photoacoustic cell chamber, causing a signal phase inversion of 180°. Analytically, this signal phase inversion is described in equation (7) through the dependence of the phase on $\tan^{-1}[1/(af^{1/2}-1)]$. For the product $af^{1/2} < 1$, the $\tan^{-1}$ is <0, while for the product $af^{1/2} > 1$, the $\tan^{-1}$ is >0, and an abrupt change in the PA signal phase is observed.

Figures 5 and 6 show the PAS signal amplitude and its phase corresponding to the first measurement for the annealed sample. All subsequent measurements for both signal amplitude and phase were identical. The PAS signal amplitude shown in figure 5 was similar to the third measurement for the as-milled sample (see figure 3). The same is also observed for the signal phases. These results suggest that the same heat transfer mechanism is present in both samples.

According to equations (4) and (5), which describe the contribution of the thermal diffusion mechanism to the PAS measurements, the 'a' value must be equal in both expressions in the same modulation frequency region. By fitting the plots of LnS versus $\sqrt{f}$ and Φ (radian) versus $\sqrt{f}$ to a straight line, the 'a' values are obtained. For the first PAS measurement of the as-milled sample (open circle line in figures 3 and 4), the best fitting for the thermal diffusion mechanism was reached in the modulation frequency interval of 15–50 Hz. Considering the plots in the order stated above, the values obtained were $a = -0.262$ and -0.261, respectively. Using the expression $a = l_s(\pi/\alpha_s)^{1/2}$, the calculated average thermal diffusivity value was $\alpha_s = 1.59 \times 10^{-5}$ m^2 s^{-1}. The PAS signal amplitude shows a modulation frequency dependence

of the type $f^{-1.0}$ after 62 Hz, where the inversion phase occurs. This indicates the presence of another dominant heat transfer mechanism contributing to the PAS signal, which may be nonradiative surface recombination and/or thermoelastic bending. The absence of nonradiative surface recombination was verified by it not being possible to fit the phase data to the phase expression given by Pinto Neto [20]. The thermal diffusivity value of $\alpha = 1.01 \times 10^{-5}$ m^2 s^{-1} reported by Sankar and Ramachandran [27] was taken as the initial value for the fitting. The absence of this mechanism may be associated with the high band gap energy value, making it difficult to promote an excess of carrier to the empty conduction band. On the other hand, the expression for the phase corresponding to the thermoelastic bending mechanism, reproduced as expression (7), was successfully fitted to the Φ (radians) versus f plot in the modulation frequency range of 65–100 Hz. From the best fit, the thermal diffusivity value of $\alpha_s = 1.65 \times 10^{-5}$ m^2 s^{-1} was obtained. This value is about 4% greater than that obtained previously. This difference may be associated with the difficulty in isolating the pure heat transfer mechanism. For the second and third PAS measurements of the as-milled sample (thick solid and open star lines in figures 3 and 4), only the thermoelastic bending mechanism was isolated in the modulation frequency range of 60–140 Hz, and 22–110 Hz, respectively. From the best fits, thermal diffusivity values of $\alpha_s = 1.49 \times 10^{-5}$ and 1.43×10^{-5} m^2 s^{-1}, respectively, were obtained.

The PAS signal of the annealed sample shows a modulation frequency dependence of the type $f^{-1.0}$ (see figure 5). Due to its similarity with that of the as-milled sample, one can infer that the thermoelastic bending contribution is the main mechanism present. Figure 6 shows the best fit of the phase data to equation (7), which gave the thermal diffusivity value of $\alpha_s = 1.05 \times 10^{-5}$ m^2 s^{-1}. This value is similar to that reported by Sankar and Ramachandran [27].

It is interesting to note that the thermal diffusivity value obtained in this study decreases with the sequence of PAS measurements of the as-milled sample. Also, a substantial reduction in the value of this parameter for the annealed sample was observed. For the as-milled sample, the decrease in the value of the thermal diffusivity can be attributed to the partial elimination of defect centers, strains and stresses, by the energy absorbed from the modulated light beam. For the annealed sample, based on the XRD and optical absorbance measurements, the substantial reduction in the thermal diffusivity value is attributed to the elimination of defect centers, strains, stresses and crystallite growth during the heat treatment. Sankar and Ramachandran [27] studied the thermal diffusivity dependence on the dislocation density. They observed a reduction in this parameter value with decreasing dislocation density. Their results support the conclusions drawn from the study here presented.

It is interesting to note from the PAS analysis that both as-milled and annealed ZnSe samples did not present the nonradiative recombination mechanism of heat transfer. It is well known that the defect centers in semiconductor materials facilitates this mechanism. Thus, we believe that the inhibition of the nonradiative recombination mechanism is related to the wide band gap energy of the ZnSe semiconductor, which limits the excitation of a great number of carriers to the conduction band.

5. Conclusions

Several conclusions were drawn from this study, the main ones being as follows.

The milling of a Zn and Se mixture, with equiatomic ZnSe composition, for 10 h resulted in a final product containing the zinc-blende ZnSe structure, in the nanostructured form. However, this as-milled product shows an important interfacial component responsible for its dark brown color. A high-quality zinc-blende ZnSe powder, maintaining the nanostructured form, was obtained after an annealing process. This annealed powder showed a yellow color as presented by commercial products.

Due to an interfacial component in the as-milled zinc-blende ZnSe powder, the absorbance spectrum showed a substantial number of defect states in the optical band gap, making the precise determination of band gap energy difficult. However, after annealing this powder, the number of defect states was substantially reduced, allowing the precise determination of the band gap energy, which was similar to the value reported in the literature.

A sequence of PAS measurements of the same as-milled zinc-blende ZnSe powder showed a change from thermal diffusion combined with a thermoelastic bending heat transfer mechanism to thermoelastic bending only. This latter mechanism is the only one found in the PAS signal amplitude for the annealed sample. A reduction in the thermal diffusivity value was observed in the sequence of PAS measurements of the same as-milled zinc-blende ZnSe powder. This reduction was attributed to the structural relaxation of defect centers with low activation energy. After a heat treatment of the as-milled zinc-blende ZnSe powder, a stable thermal diffusivity value was obtained for a sequence of PAS measurements of the annealed sample. This value is in agreement with that reported in the literature.

Acknowledgments

We are grateful to the Brazilian agencies CNPq, FAPESC and FINEP for financial support. We thank to the Laboratório de Caracterização Microestrutural(LCM) from UFSC for SEM and EDX measurements.

References

[1] Che J, Yao X, Jian H and Wang M 2004 *Ceram. Int.* **30** 1935
[2] Gleiter H 1992 *Nanostruct. Mater.* **1** 1
[3] Stern E A, Siegel R W, Newville M, Sanders P G and Haskel D 1995 *Phys. Rev. Lett.* **75** 3874
[4] Boldish S I and White W B 1998 *Am. Mineral.* **83** 865
[5] Balasubramaniam A K, Sankar N, Ramakrishnan S K and Ramachandran K 2004 *Cryst. Res. Technol.* **39** 558
[6] Gallian A, Fedorov V V, Mirov S B, Badikov V V, Galkin S N, Voronkin E F and Lalayants A I 2006 *Opt. Express* **14** 11694

[7] Leppert V J, Mahamuni S, Kumbhojkar N R and Risbud S H 1989 *Mater. Sci. Eng.* B **52** 89
[8] Ekimov A I and Onushchenko A A 1984 *JETP Lett.* **40** 1136
[9] Borrelli N F, Hall D W, Holland H J and Smith D W 1987 *J. Appl. Phys.* **61** 5399
[10] Potter B G and Simmons J H 1988 *Phys. Rev.* B **37** 10838
[11] Liu L C and Risbud S H 1990 *J. Appl. Phys.* **68** 28
[12] Nogami M, Nagaska K and Kato E 1990 *J. Am. Ceram. Soc.* **73** 2097
[13] Suryanarayana C 2001 *Prog. Mater. Sci.* **46** 1
[14] de Lima J C, dos Santos V H F and Grandi T A 1999 *Nanostruct. Mater.* **11** 51
[15] Machado K D, de Lima J C, de Campos C E M, Grandi T A and Gasperini A A M 2003 *Solid State Commun.* **127** 477
[16] Stucky G D and Macdougall J E 1990 *Science* **247** 669
[17] de Lima J C, Cella N L, Miranda L C M, An Chying C, Franzan A H and Leite N F 1992 *Phys. Rev.* B **46** 14186
[18] Rosencwaig A and Gersho A 1976 *J. Appl. Phys.* **47** 64
[19] Ziegler G and Hasselman D P H 1981 *J. Mater. Sci.* **16** 495
[20] Pinto Neto A, Vargas H, Leite N F and Miranda L C M 1990 *Phys. Rev.* B **41** 9971
[21] de Lima J C, Schmitt M, Souza S M, Almeida T O, Jerônimo A R, Trichês D M, Grandi T A and Campos C E M 2007 *J. Alloys Compounds* **436** 13
[22] Shang S, Wang Y, Liu Z, Yang C and Yin S 2007 *Appl. Phys. Lett.* **91** 23115
[23] Tanusevski V G A 2003 *BPU-5: 5th General Conf. Balkan Physical Union (Vrnjaeka Banja, Aug)*
[24] JCPDS-Powder Diffraction File System Manual. International Center for diffraction Data 1996 Pennsylvania, USA
[25] Rietveld H M 1965 *J. Appl. Crystallogr.* **2** 65
[26] Strnad Z 1986 *Glass-Ceramic Materials, Glass Science and Technology* vol 8 (Amsterdam: Elsevier) p 161
[27] Sankar N and Ramachandran K 2003 *J. Cryst. Growth* **247** 157
[28] Rousset G, Lepoutre L and Bertrand L 1983 *J. Appl. Phys.* **54** 2383
[29] Kolobov A, Fons P, Frenkel A I, Ankudinov A L, Tominaga J and Uruga T 2004 *Nat. Mater.* **3** 703